Three-fold covariance imaging of laser-induced Coulomb explosions

James D. Pickering,[1, a)] Kasra Amini,[1] Mark Brouard,[1, b)] Michael Burt,[1] Ian J. Bush,[2] Lauge Christensen,[3] Alexandra Lauer,[4] Jens H. Nielsen,[3, c)] Craig S. Slater,[4] and Henrik Stapelfeldt[5, d)]

[1)] *The Chemistry Research Laboratory, Department of Chemistry, University of Oxford, 12 Mansfield Road, Oxford, OX1 3TA, United Kingdom*

[2)] *Oxford e-Research Centre, 7 Keble Road, Oxford, OX1 3QG, United Kingdom*

[3)] *Department of Physics and Astronomy, Ny Munkegade 120, Aarhus University, DK-8000 Aarhus C, Denmark*

[4)] *Department of Chemistry, University of Oxford, The Physical and Theoretical Chemistry Laboratory, South Parks Road, Oxford, OX1 3QZ, United Kingdom*

[5)] *Department of Chemistry and Interdisciplinary Nanoscience Center (iNANO), Langelandsgade 140, Aarhus University, DK-8000 Aarhus C, Denmark*

(Dated: 12 April 2016)

We apply a three-fold covariance imaging method to analyse previously acquired data [Phys. Rev. A 89, 011401(R), (2014)] on the femtosecond laser-induced Coulomb explosion of spatially pre-aligned 3,5-dibromo-3′,5′-difluoro-4′-cyanobiphenyl molecules. The data were acquired using the 'Pixel Imaging Mass Spectrometry' (PImMS) camera. We show how three-fold covariance imaging of ionic photofragment recoil trajectories can be used to provide new information about the parent ion's molecular structure prior to its Coulomb explosion. In particular, we show how the analysis may be used to obtain information about molecular conformation, and provides an alternative route to enantiomer determination.

PACS numbers: 33.80.Gj, 33.15.Hp, 33.80.Rv, 34.50.Gb, 42.50.Hz
Keywords: Coulomb explosion imaging, covariance imaging, fast imaging sensor

Covariance is a statistical measure of the degree of correlation between two or more random variables,[1] and can reveal correlations that are otherwise hidden in raw data. Covariance mapping by plotting a matrix of covariance values is an intuitive way to represent covariance data, as it allows correlations to be clearly observed by examining the relative magnitudes of adjacent matrix elements. Covariance mapping was first applied to molecular dynamics experiments by Frasinski *et al.*,[2] to reveal correlations between mass peaks in one-dimensional (1D) time-of-flight (ToF) spectra. Since then, both two- and three-variable covariance mapping have been applied to 1D ToF data for a variety of different systems.[3,4] Covariances between mass peaks in a ToF spectrum reveal which products are formed from the same dissociation pathway, for example, but in general provide only limited information on more detailed dynamics, such as correlations between photofragment recoil velocities. We investigate the latter using Coulomb explosion imaging (CEI).

Coulomb explosion is the process that occurs when several electrons are rapidly removed from a molecule, resulting in the fragmentation of the molecule into cationic fragments. The nascent fragments can be velocity mapped onto a two-dimensional (2D) imaging detector. If the Coulomb explosion occurs on a faster timescale than the vibrational motion of the target molecule, then the ion positions mapped on the 2D detector often approximately reflect the initial positions of the atoms at the point of explosion. This is the principle of CEI.

Coulomb explosion can be induced either by irradiation with intense femtosecond laser pulses,[5–7] or by the collision of a fast beam of molecular ions with a thin metal foil.[8] Laser based Coulomb explosion is the most widely used method, and the one employed in this work.

In the data employed in the work described here, the 'Pixel Imaging Mass Spectrometry' (PImMS) camera[9–11] is used to record (x, y) pixel coordinates and characteristic time-stamps for each detected ion produced in an experimental cycle. Covariances between PImMS pixel events can be calculated, and the resulting correlations between fragment momenta can be plotted as a covariance map. Applying covariance mapping to imaging data in this way is referred to as covariance imaging, and has been demonstrated for two-fragment correlations.[7,12,13] 2D covariance imaging has been shown to provide a wealth of dynamical information beyond that provided by direct 2D ion images and conventional ToF covariance mapping.[14] Here we extend this analysis technique to three-fragment correlations, and show that this further enhances the power of the covariance imaging technique. In particular, we show how the analysis allows a direct determination of the absolute configuration of a chiral molecule in the gas phase - a subject of considerable current interest and activity.[15,16]

The data set used to illustrate the three-fold covariance technique in this study involved the Coulomb explosion of 3,5-dibromo-3′,5′-difluoro-4′-cyanobiphenyl (BFCbP).

[a)] Current address: Department of Chemistry, Langelandsgade 140, Aarhus University, DK-8000 Aarhus C, Denmark
[b)] Electronic mail: mark.brouard@chem.ox.ac.uk
[c)] Current address: Research Software Development Group, Research IT Services, University College London, Podium Building (1st Floor), Gower Street, London, WC1E 6BT, United Kingdom
[d)] Electronic mail: henriks@chem.au.dk

This data set has previously been subject to two-fold covariance imaging by Slater *et al.*[7,12] The experimental setup used to obtain the data has been described previously in detail,[5,7,12] with only pertinent details covered here.

A cold molecular beam of BFCbP was produced *via* supersonic expansion through an Even-Lavie valve, and then collimated through two skimmers. The beam subsequently passed through an electrostatic deflector that deflected molecules in the lowest lying rotational states towards the target chamber.[17] The molecules were then intersected by two different pulsed laser beams. First, a 10 ns linearly polarized pulse from a Nd:YAG laser was used to induce adiabatic 1D alignment (1064 nm, 8×10^{11} W cm^{-2}) of the molecule's most polarisable axis (MPA, the stereogenic axis) either parallel or perpendicular to the plane of the detector, depending on the polarisation of the laser field. Second, an intense 30 fs pulse from a Ti:Sapphire laser (800 nm, 3×10^{14} W cm^{-2}), polarised parallel to the alignment pulse polarisation, induced Coulomb explosion in the target molecule. The nascent ions were then velocity-mapped onto an MCP/P47 phosphor ion imaging detector, with the flashes of light from the phosphor imaged onto the PImMS camera. For each laser shot, the camera recorded the flash events on a pixel-by-pixel basis in the form of a series of (x, y, t) time-stamps, which were then stored for subsequent analysis.[7,12,13]

Three-fold covariance is described mathematically through the expression[1,18]

$$\begin{aligned}\mathrm{cov}(X,Y,Z) = \langle XYZ\rangle - \langle XY\rangle\langle Z\rangle - \langle XZ\rangle\langle Y\rangle \\ - \langle YZ\rangle\langle X\rangle + 2\langle X\rangle\langle Y\rangle\langle Z\rangle\,, \end{aligned} \quad (1)$$

where the terms $\langle X\rangle$, $\langle XY\rangle$, and $\langle XYZ\rangle$ are defined

$$\langle X\rangle = \frac{1}{N_\mathrm{S}}\sum_{i=1}^{N_\mathrm{S}} X_i(x) \quad (2)$$

$$\langle XY\rangle = \frac{1}{N_\mathrm{S}}\sum_{i=1}^{N_\mathrm{S}} X_i(x)Y_i(y) \quad (3)$$

$$\langle XYZ\rangle = \frac{1}{N_\mathrm{S}}\sum_{i=1}^{N_\mathrm{S}} X_i(x)Y_i(y)Z_i(z)\,. \quad (4)$$

These terms represent the expectation values of observing ion X alone, ions X and Y in two-fold coincidence, and ions X, Y, and Z in three-fold coincidence respectively, where N_S is the number of laser shots sampled, and $X_i(x)$ represents the ion event x, recorded in laser shot i produced at pixel coordinate X_i. Thus, counting the number of two-fold and three-fold coincidence events present in a data set allows the three-fold covariance image to be produced. The validity of three-fold covariance mapping has previously been discussed by Zhaunerchyk *et al.*.[18] There it was established that a three-fold covariance map can be interpreted in the same way as a two-fold covariance map, provided that the number of fragmentation events per laser shot varies with Poisson statistics.

The three-fold covariance images shown herein are 'recoil frame' covariance images,[7] which have been extensively described for two-ion correlations by Slater *et al.*.[7,12] For three ions, a recoil-frame covariance image is constructed with one ion designated a 'reference' ion, one a 'constrained' ion, and the final ion plotted in the frame of the reference ion. To achieve this, the velocity vectors of the reference ion are rotated and summed into a single vector, with the velocity vectors of the other two ions plotted relative to this vector. The 'constrained' ions can then have their velocity vectors selected to be in a certain area of the covariance image. This makes it possible to plot covariances between three ions, where one is oriented along a single vector (reference), and another is constrained to recoil in a certain area (constrained). This effectively allows control of two velocity vectors, which provides a greater effective constraint on the orientation of the parent molecule that is imaged. An illustration of the steps involved in this process is shown in Fig. 1.

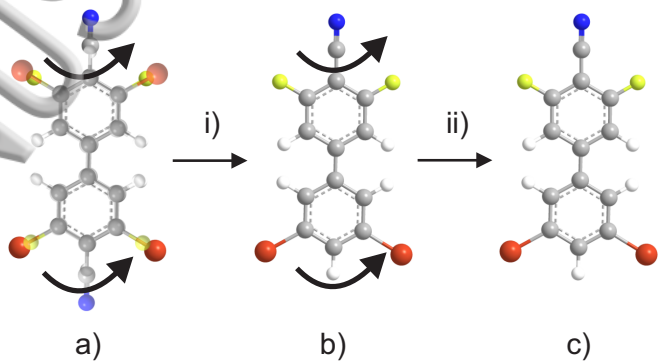

FIG. 1. Demonstration of the utility of covariance imaging. Before any covariance analysis (a), the molecule is 1D aligned in space (but not oriented) and is free to rotate about the MPA. After two-fold covariance analysis (i), the molecule is artificially oriented, but can still rotate (b). After three-fold covariance analysis (ii), the molecule is artificially oriented, and the rotation is restricted by constraining a second vector (c). The color coding of the atoms in the various panels is Br (large red), F (small yellow), N (small blue), H (small white), and C (small grey).

Computationally, the data are processed as follows. The raw data in an (x, y, t, i) format are read in and sorted by laser shot number i. Each line of data represents an ion event, and all events occurring in the first laser shot are listed first, followed by events occurring in the second laser shot, and so on. The covariance map is then built up as a sum of coincidences according to Eq. (1). Coincidences are found by reading the first ion event, and then finding every event that occurs in the same laser shot as this initial event. When no more coincident events are found, the initial event is stepped on to the second recorded ion event, and every sequential event is again checked so that every coincident event is

found. This process is repeated until all coincidences are found. When a coincidence is found, it is scaled by a factor of $\frac{1}{N_S}$ and the coincidence is transformed into the recoil frame. It is then added to or subtracted from the final covariance matrix as necessary to build up a full three-fold covariance image.

Fig. 2 shows three-fold covariance images with BFCbP aligned with the MPA parallel to the detector plane. As discussed, the events shown are three-ion correlations, with the position of the constrained ion relative to the reference denoted by the highlighted area in grey. The covariance images show three-ion correlations between Br^+, F^+ and N^+. In each panel, the distribution plotted is the N^+ recoil velocity, with Br^+ as the reference fragment, and F^+ as the third fragment, either unconstrained (top panel of Fig. 2), or constrained to the specific area defined on the left (middle panel) or the right (bottom panel). Thus, the images show where N^+ is likely to recoil, given it recoils together with a Br^+ and an F^+ ion.

The top frame of Fig. 2 shows the three-fold covariance image without a constraint placed on the F^+ recoil velocity. The N^+ distribution in this case is found to be symmetric, and is similar to the distribution observed from a two-ion covariance image between Br^+ and N^+ for this same system.[7,12] This behavior is as expected; if the F^+ can recoil in any direction, there are two distinct orientations of the molecule that can be imaged. The N^+ can recoil in the bottom-left or bottom-right quadrant: the two orientations that give rise to this distribution are shown in the ball-and-stick models to the right of the covariance maps. The middle and bottom frames illustrate the utility of the three-fold covariance imaging technique, as here the F^+ recoil velocity is confined either to the left or right of the image. The ball-and-stick models show that by constraining the F^+ in this way, it is possible to image one of the two possible orientations of the molecule, or, indeed, alternatively, to determine the mutual orientation of the various substituents in the parent molecule prior to Coulomb explosion. For example, constraining F^+ to the left selects out only the molecules where N^+ is recoiling to the bottom left (and vice versa). The reason for this is clear from the ball-and-stick model. If F^+ is confined to the left, given the structure of the parent molecule it is impossible to have an N^+ recoiling to the bottom right. This is observed in the covariance images, where the distribution is no longer symmetric, as one specific orientation of the parent molecule has effectively been imaged in each case.

Fig. 3 shows three-fold covariance images with BFCbP aligned with the MPA perpendicular to the detector plane. The correlations imaged for this geometry are between Br^+ (reference fragment) and both F^+ fragments (one F^+ can be constrained and the other plotted). The three images shown are with F^+ unconstrained (top) and with F^+ constrained to the top left and top right (middle and bottom respectively). Importantly, for this example, the F^+ is also confined in ToF to be the F^+ scattered 'forwards', towards the detector face (as the forward and

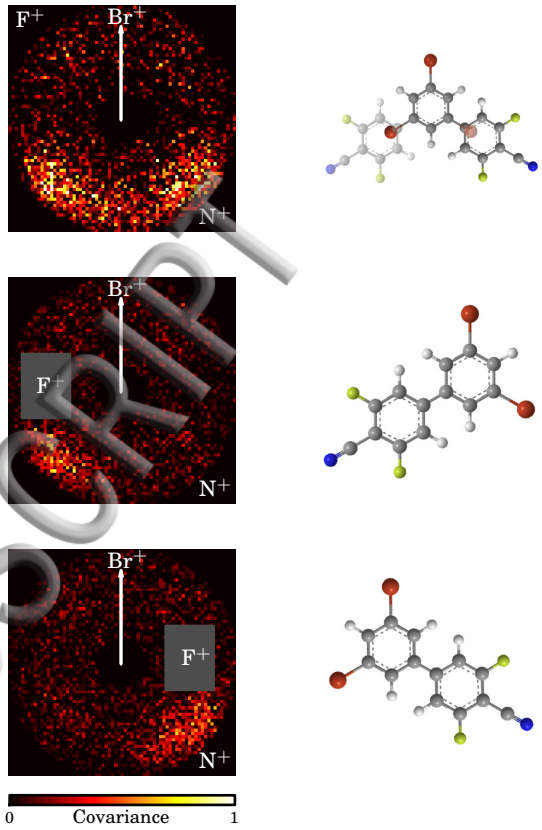

FIG. 2. Three-fold covariance images of BFCbP, aligned parallel to the detector plane. The images show the three-ion covariance image between Br^+, F^+ , and N^+ with the F^+ recoil velocity unconstrained (top), constrained left (middle), and constrained right (bottom). The right panels show the parent molecules in the appropriate orientation, with atoms color coded as in Fig. 1. Each covariance image has been normalised such that the values for each element lie between 0 and 1.

back scattered F^+ are clearly resolved in ToF).[7,12,13] This has the effect of *orienting* the molecules with the CN group pointing 'towards' the detector face, which would not be possible by use of the 1D alignment pulse alone. The angular distributions are shown with both the raw data (black line), and after smoothing (red line).

BFCbP is an axially chiral molecule, with two enantiomeric forms having a torsion angle of ±39°, as shown in Fig. 4. The top-most covariance image shows four-fold symmetry, resulting from both enantiomers being imaged simultaneously (as illustrated in the ball-and-stick molecule on the right of the image). Using three-fold covariance, it is possible to image each enantiomer separately by constraining one of the F^+ fragments to a specific area. This is shown in the covariance images in the middle and bottom panels of Fig. 3, which demonstrate

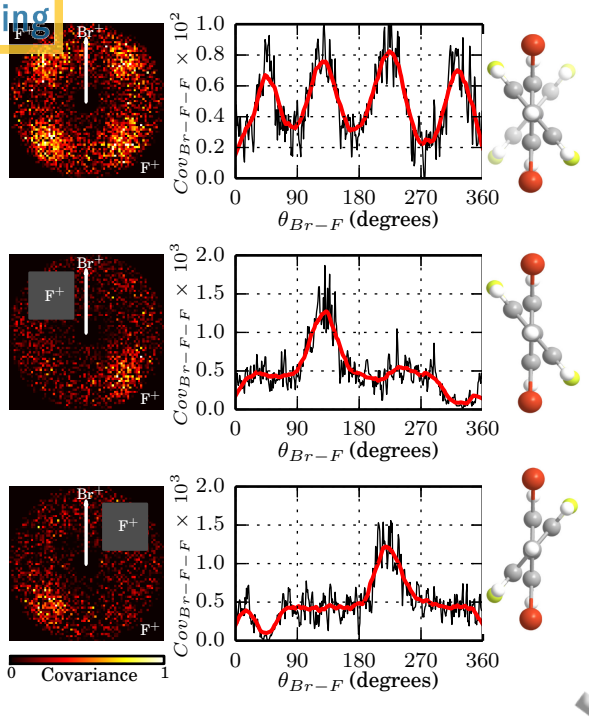

FIG. 3. Three-fold covariance images of BFCbP, aligned perpendicular to the detector plane. The images show the three-fold covariance between Br^+ and both F^+ fragments, with one F^+ fragment unconstrained (top), constrained right (middle), and constrained left (bottom). The right panels show the parent molecules in the appropriate orientation, with atoms color coded, and images normalised as in Fig. 1. The bottom two panels show a dip in the angular distribution at around 321° and 39° respectively, which is due to the subtraction of the auto-correlation between the constrained F^+ ion and itself.

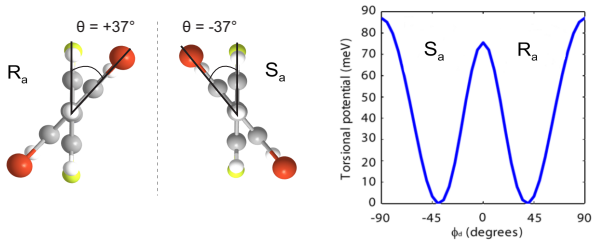

FIG. 4. The torsional potential of BFCbP (right panel), with a ball-and-stick model of the two enantiomeric forms (left panel). In the latter, the atoms are color coded as in Fig. 1.

the imaging of the R (middle) and S (bottom) enantiomers separately. Whilst such selective fragment imaging may also be achieved in the low count rate regime using coincidence techniques such as COLTRIMS,[6] it is not possible using two-fold covariance imaging. Three-fold covariance imaging overcomes the limitations of two-fold covariance, and also removes the need for low ion flux and high repetition rate demanded by coincidence techniques.

It is clear from the covariance images and angular intensity distributions that there is a certain level of background intensity and noise present in the three-fold covariance images. This noise, which arises from the statistical nature of the covariance analysis, could be problematic if a quantitative measure of enantiomeric excess or purity was desired for the gas phase molecule. Because covariance analysis is a statistical measure of the correlation between two or more variables, a larger number of sampling points will increase the statistical precision (and reduce the level of noise). In this specific case, a larger number of laser shots will increase the size of the data set (*i.e.* the total number of recorded ion events), and reduce the level of noise. It is clear from the plots in Fig. 3 that there is a greater background intensity in the plots with a constrained F^+ fragment. This is a result of the three-fold procedure: by constraining the recoil velocity of F^+ to a smaller area, events in which F^+ recoils into other areas are discarded. Additionally, by only selecting molecules where the CN group is oriented towards the detector, data is discarded in a similar way. Thus, the effective number of recorded ion events the covariance analysis is run with is reduced if an ion is constrained to a particular region of the image. This can be remedied by increasing the data acquisition time in the experiment, thereby recording more events to compensate for those which are discarded in the constraining process. However, it is possible to approximate these increased statistics using an averaging procedure, the results of which are shown in Fig. 5.

The averaged images shown in Fig. 5 are a sum of four individual covariance images. The image shown to the left of the top-most panel comprises a sum of the following four images: 1) the original image of the S enantiomer (forward scattered molecules); 2) a reflected image of the R enantiomer (forward scattered molecules); 3) the image of the R enantiomer (backward scattered molecules); and 4) a reflected image of the S enantiomer (backward scattered molecules). It is clear from the covariance images and angular intensity distributions that this increases the contrast between signal and background, as there is greater statistical precision for these summed images. These images show the effect that an increased data acquisition time would have on the overall covariance images. It is clear that the contrast is improved with this full averaging procedure. The result of this is that it is possible to image the absolute chirality of an axially chiral molecule in the gas phase, using three-fold covariance imaging.

We have demonstrated that it is possible to extend the two-fold covariance image analysis using PImMS data, originally developed by Slater *et al.*,[7,12,19] to a corresponding three-fold covariance imaging method based on the theoretical work of Zhaunerchyk *et al.*.[18] Previous three-fold correlation techniques have been limited either to coincidence analysis,[6,20] which require a very low

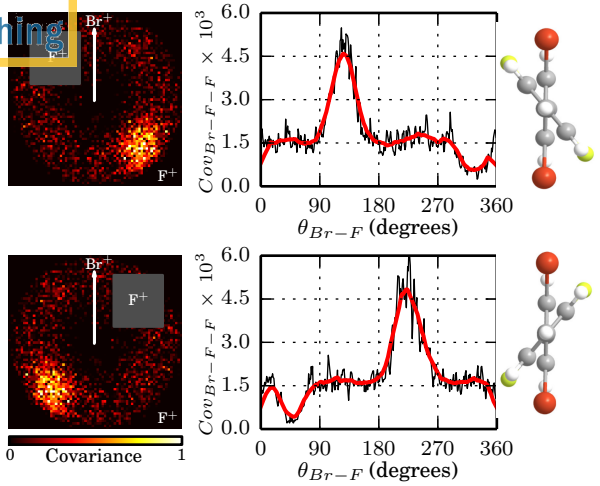

FIG. 5. Three-fold covariance images of BFCbP, aligned perpendicular to the detector plane. These show the same covariances as the images in figure 3, but the images shown here are averaged figures showing that it is possible to reduce the background intensity using an averaged procedure. The right panels show the parent molecules in the appropriate orientation, with atoms color coded and images normalised as in Fig. 1. Autocorrelations are subtracted as in Fig. 3.

ion flux to observe true correlations, or to three-fold covariance mapping of mass peaks in 1D ToF spectra.[3,21] The present study extends this work by demonstrating the imaging of individual enantiomers of an axially chiral substituted biphenyl molecule in the gas phase, using three-fold covariance imaging, thus providing an alternative to coincidence techniques that is not limited by ion flux or repetition rate constraints.

ACKNOWLEDGMENTS

H.S. acknowledges an ERC-AdG (Project No. 320459 – DropletControl), The Lundbeck Foundation, The Carlsberg Foundation, and The Danish Council for Independent Research (Natural Sciences). M.B. and J.D.P. thank John H.D. Eland for valuable discussions. M.B. acknowledges the support of the EPSRC *via* Programme Grants No. EP/L005913/1 and EP/G00224X/1, the EU through grant FP7 ITN "ICONIC" (Project Grant No. 238671), STFC through a PNPAS award and a mini-IPS grant (ST/J002895/1), and a proof of concept grant from ISIS Innovation Ltd.. A.L. thanks the DFG through Grant Nos. LA 3209/1-1 and LA 3209/1-2, for support. J.D.P. would like to acknowledge the use of the University of Oxford Advanced Research Computing (ARC) facility in carrying out this work: http://dx.doi.org/10.5281/zenodo.22558.

[1] W. J. Krzanowski, *Principles of Multivariate Analysis* (Oxford University Press, New York, 1998) p. Chap. 7.1.
[2] L. J. Frasinski, K. Codling, and P. A. Hatherly, Science **246**, 1029 (1989).
[3] K. Codling and L. J. Frasinski, J. Phys. B: At., Mol. and Opt. Phys. **26**, 783 (1999).
[4] W. A. Bryan, W. R. Newell, J. H. Sanderson, and A. J. Langley, Phys. Rev. A **74**, 1 (2006).
[5] J. L. Hansen, J. H. Nielsen, C. B. Madsen, A. T. Lindhardt, M. P. Johansson, T. Skrydstrup, and H. Madsen, L. B.and Stapelfeldt, J. Chem. Phys. **136** (2012).
[6] M. Pitzer, M. Kunitski, A. Johnson, T. Jahnke, H. Sann, F. Sturm, L. P. H. Schmidt, H. Schmidt-Bocking, R. Dorner, J. Stohner, J. Kiedrowski, M. Reggelin, S. Marquardt, A. Scheisser, R. Berger, and M. S. Schoeffler, Science **341** (2013).
[7] C. S. Slater, S. Blake, M. Brouard, A. Lauer, C. Vallance, J. J. John, R. Turchetta, A. Nomerotski, L. Christensen, J. H. Nielsen, M. P. Johansson, and H. Stapelfeldt, Phys. Rev. A **89**, 1 (2014).
[8] Z. Vager, R. Naaman, and E. P. Kanter, Science **244**, 427 (1989).
[9] A. Nomerotski, M. Brouard, E. Campbell, A. Clark, J. Crooks, J. Fopma, J. J. John, A. J. Johnsen, C. S. Slater, R. Turchetta, C. Vallance, E. Wilman, and W. H. Yuen, J. Inst. **5**, C07007 (2010).
[10] A. Nomerotski, S. Adigun-Boaye, M. Brouard, E. Campbell, A. T. Clark, J. Crooks, J. J. John, A. J. Johnsen, C. S. Slater, R. Turchetta, C. Vallance, E. Wilman, and W. H. Yuen, Nucl. Instrum. Methods Phys. Res. A **633**, S243 (2011).
[11] J. J. John, M. Brouard, A. Clark, J. Crooks, E. Halford, L. Hill, J. W. L. Lee, A. Nomerotski, R. Pisarczyk, I. Sedgwick, C. S. Slater, R. Turchetta, C. Vallance, E. Wilman, B. Winter, and W. H. Yuen, J. Inst. **7**, C08001 (2012).
[12] C. S. Slater, S. Blake, M. Brouard, A. Lauer, C. Vallance, C. S. Bohun, L. Christensen, J. H. Nielsen, M. P. Johansson, and H. Stapelfeldt, Phys. Rev. A **91**, 1 (2015).
[13] L. Christensen, J. H. Nielsen, C. S. Slater, A. Lauer, M. Brouard, and H. Stapelfeldt, Phys. Rev. A **92** (2015).
[14] L. Christensen, J. H. Nielsen, C. B. Brandt, C. B. Madsen, L. B. Madsen, C. S. Slater, A. Lauer, M. Brouard, M. P. Johansson, B. Shepperson, and H. Stapelfeldt, Phys. Rev. Lett. **113**, 073005 (2014).
[15] D. Patterson, M. Schnell, and J. M. Doyle, Nature **497**, 475 (2013).
[16] M. H. M. Janssen and I. Powis, Phys. Chem. Chem. Phys. **16**, 856 (2014).
[17] F. Filsinger, J. Küpper, G. Meijer, L. Holmegaard, J. H. Nielsen, I. Nevo, J. L. Hansen, and H. Stapelfeldt, J. Chem. Phys. **131**, 064309 (2009).
[18] V. Zhaunerchyk, L. J. Frasinski, J. H. D. Eland, and R. Feifel, Phys. Rev. A **89**, 1 (2014).
[19] C. S. Slater, *Studies of Photoinduced Molecular Dynamics Using a Fast Imaging Sensor*, Ph.D. thesis, University of Oxford (2013).
[20] J. H. D. Eland, P. Linusson, M. Mucke, and R. Feifel, Chem. Phys. Lett. **548**, 90 (2012).
[21] L. Frasinski, P. Hatherly, and K. Codling, Phys. Lett. A **156**, 227 (1991).

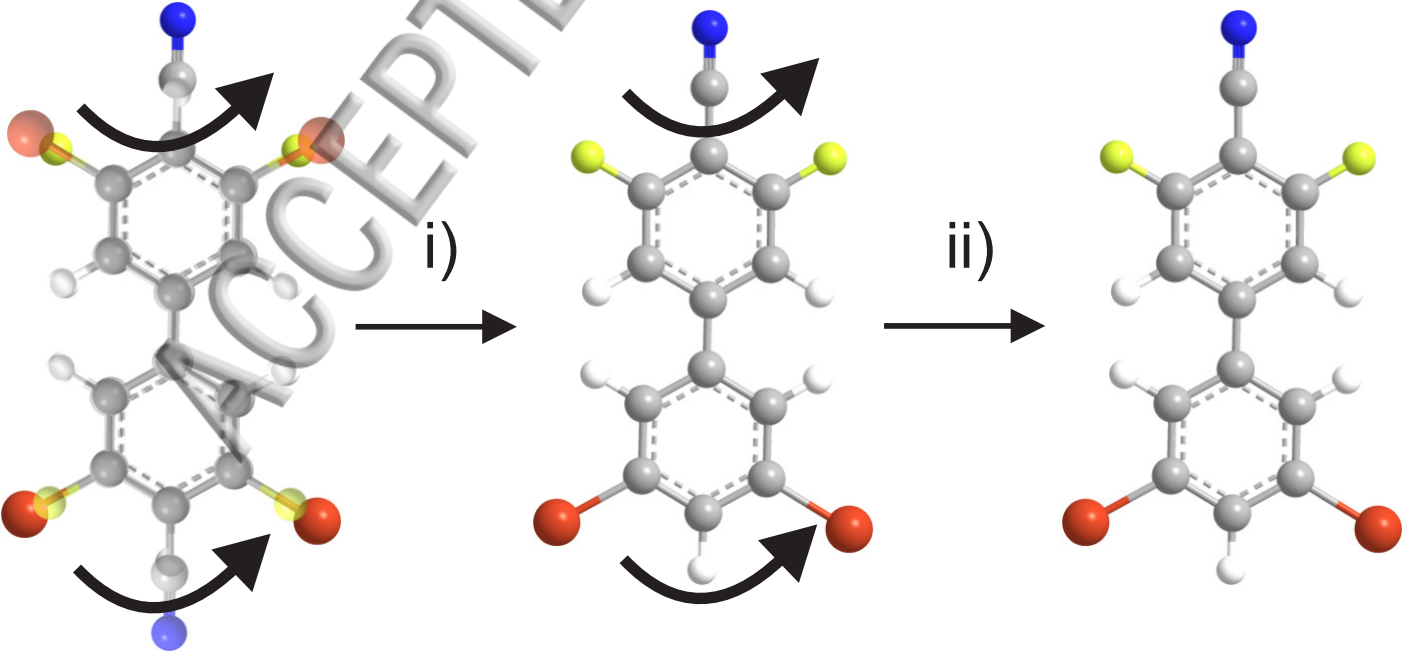

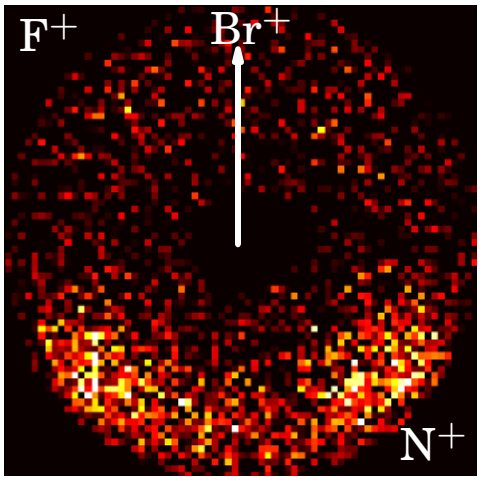

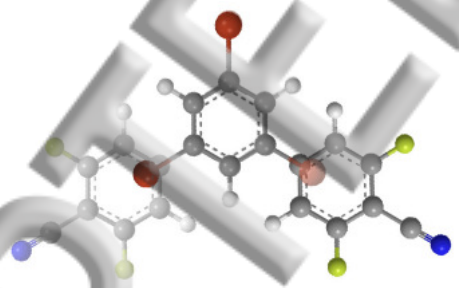

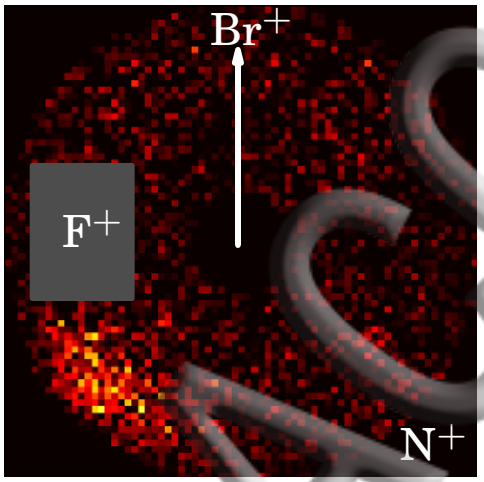

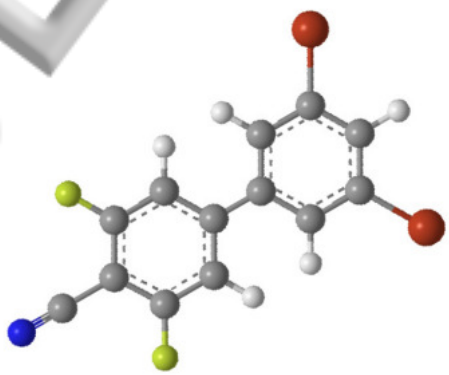

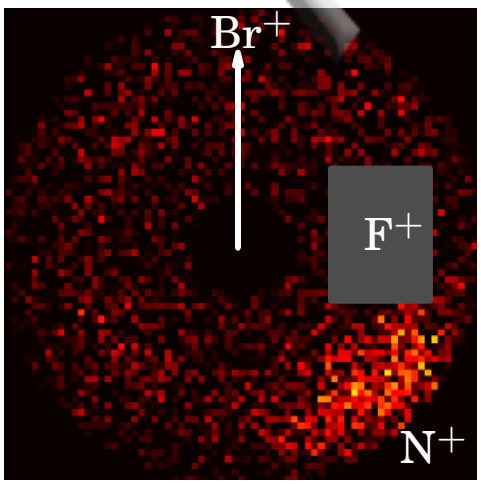

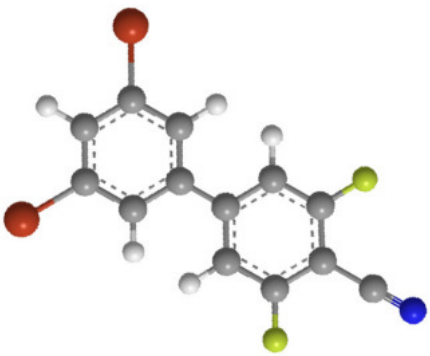

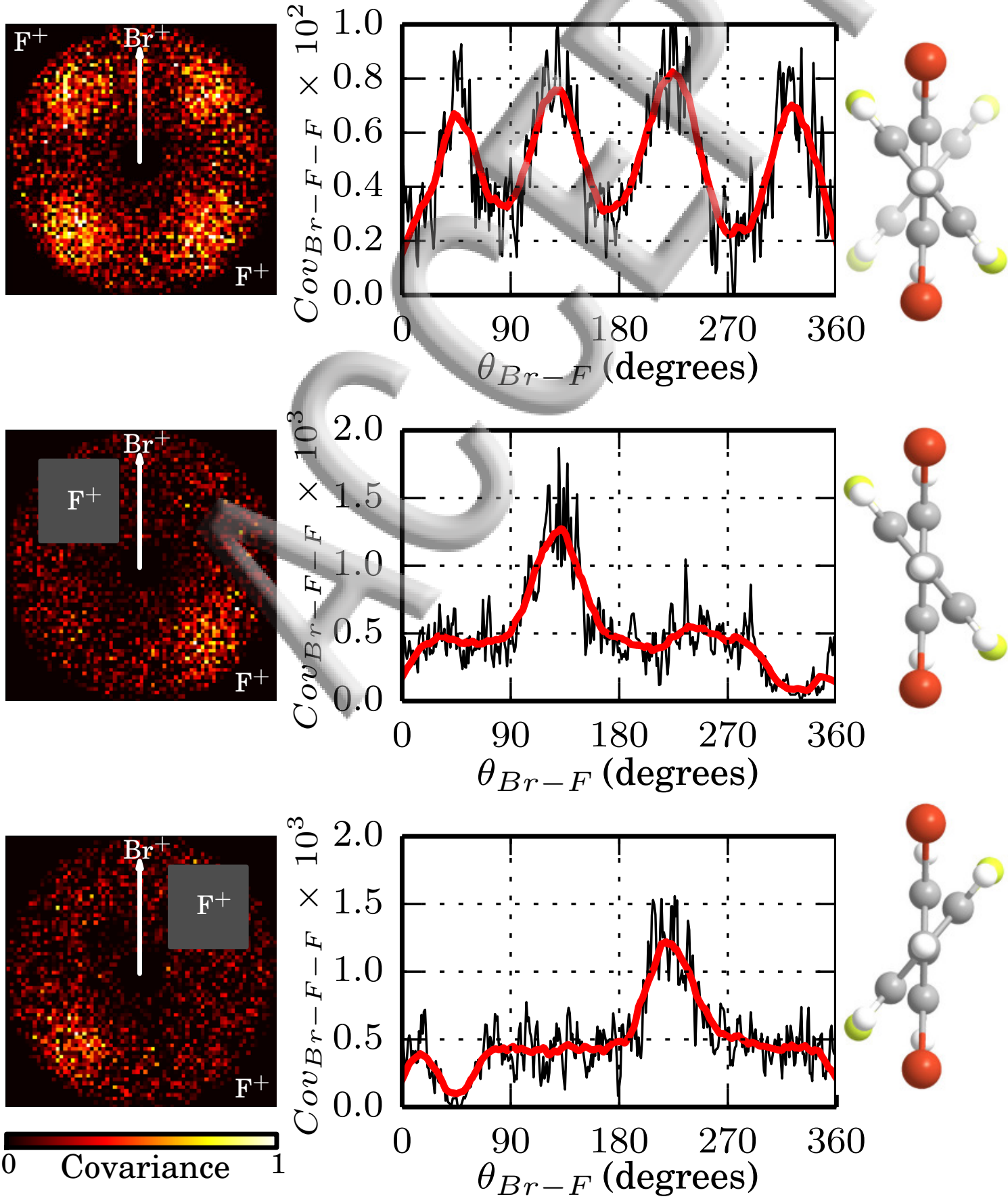
F+
Br+
F+
1.0
0.8
0.6
0.4
0.2
0.0
$Cov_{Br-F-F} \times 10^2$
0
90
180
270
360
θ_{Br-F} (degrees)
Br+
F+
F+
2.0
1.5
1.0
0.5
0.0
$Cov_{Br-F-F} \times 10^3$
0
90
180
270
360
θ_{Br-F} (degrees)
Br+
F+
F+
2.0
1.5
1.0
0.5
0.0
$Cov_{Br-F-F} \times 10^3$
0
90
180
270
360
θ_{Br-F} (degrees)
0
Covariance
1

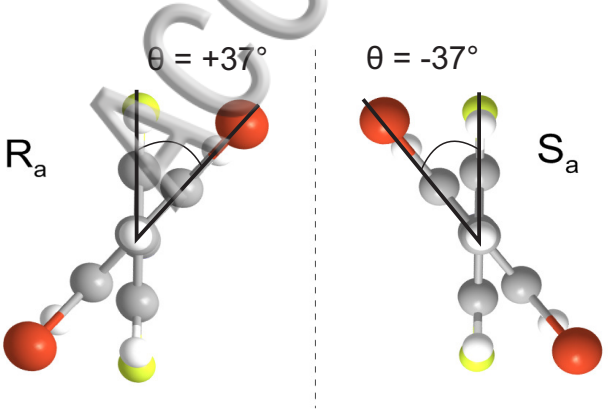
θ = +37°
θ = -37°
R_a
S_a

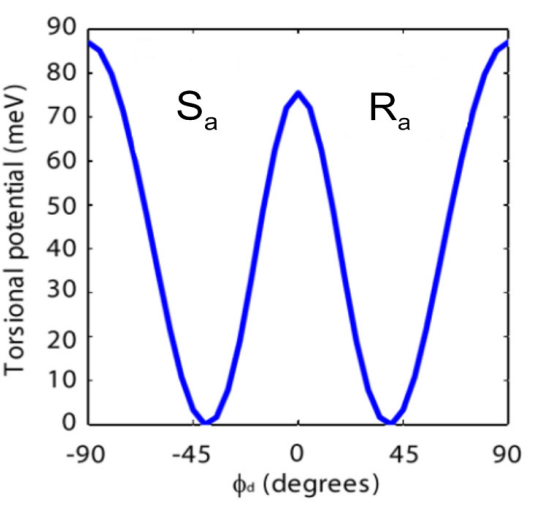
S_a
R_a
Torsional potential (meV)
90
80
70
60
50
40
30
20
10
0
-90
-45
0
45
90
ϕ_d (degrees)

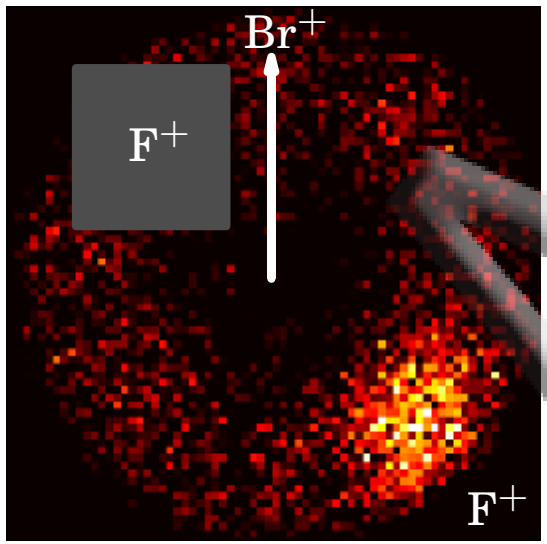
Br+
F+
F+

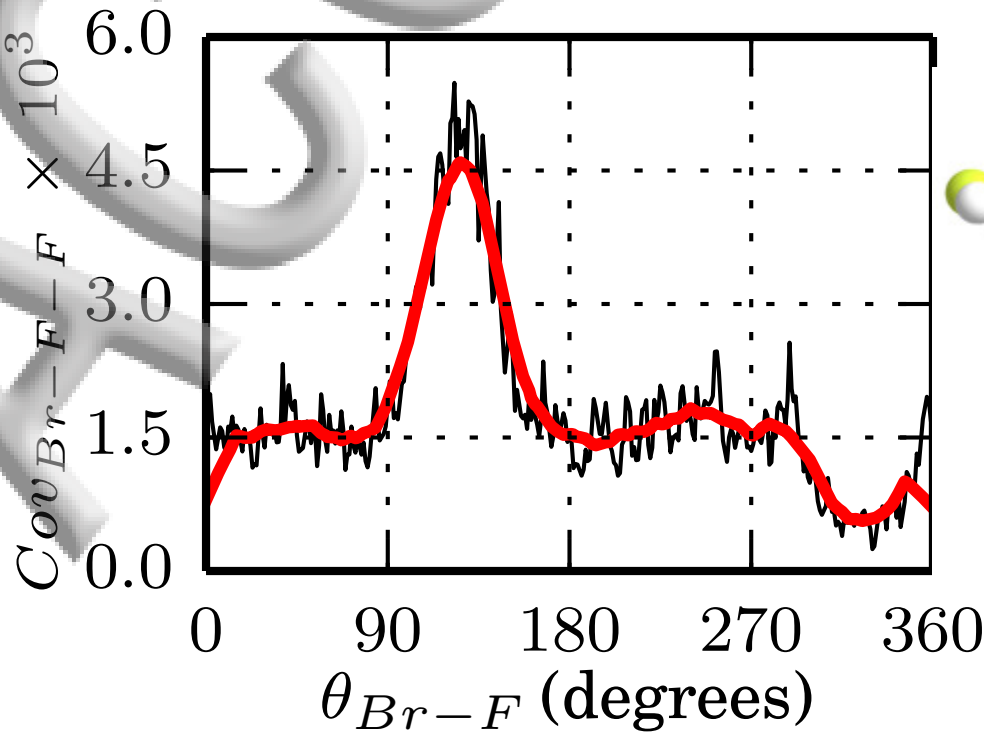
6.0
4.5
3.0
1.5
0.0
× 10^3
Cov_Br−F−F
0
90
180
270
360
θ_Br−F (degrees)

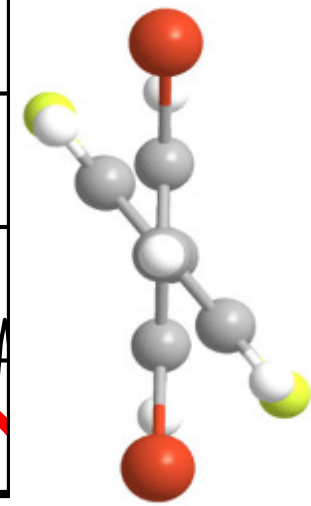

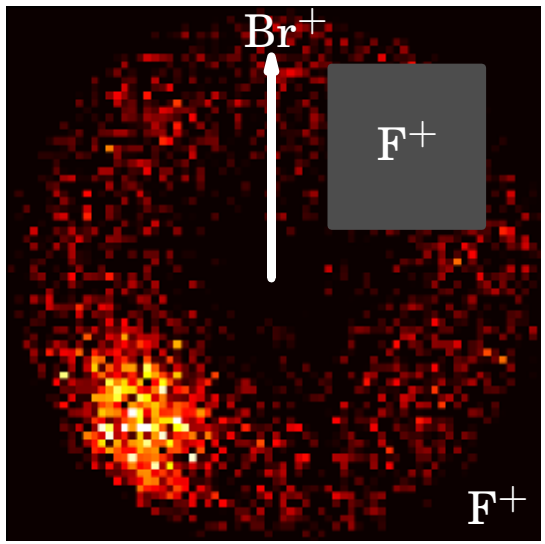
Br+
F+
F+


0
Covariance
1

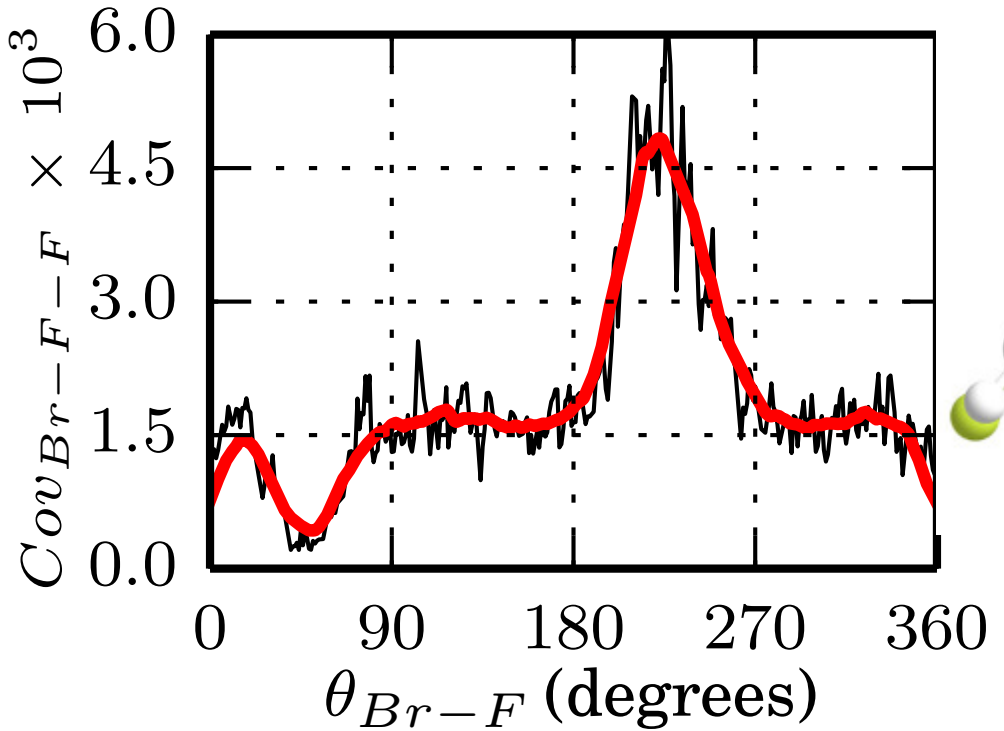
6.0
4.5
3.0
1.5
0.0
× 10^3
Cov_Br−F−F
0
90
180
270
360
θ_Br−F (degrees)